
FMM-NET: NEURAL NETWORK ARCHITECTURE BASED ON THE FAST MULTIPOLE METHOD

Daria Sushnikova

Skolkovo Institute of Science and Technology
Moscow, Russia, 143026
d.sushnikova@skoltech.ru

Pavel Kharyuk

Skolkovo Institute of Science and Technology
Moscow, Russia, 143026
Marchuk Institute of Numerical Mathematics of the Russian Academy of Sciences
Moscow, Russia, 119991
kharyuk.pavel@gmail.com

Ivan Oseledets

Skolkovo Institute of Science and Technology
Moscow, Russia, 143026
Marchuk Institute of Numerical Mathematics of the Russian Academy of Sciences
Moscow, Russia, 119991
ivan.oseledets@gmail.com

ABSTRACT

In this paper, we propose a new neural network architecture based on \mathcal{H}^2 matrix. Even though networks with \mathcal{H}^2 -inspired architecture already exists, and our approach is designed to reduce memory costs and improve performance by taking into account the sparsity template of \mathcal{H}^2 matrix. In numerical comparison with alternative neural networks, including the known \mathcal{H}^2 based ones, our architecture showed itself as beneficial in terms of performance, memory, and scalability.

1 INTRODUCTION

Neural networks (NN) have become extremely popular in the recent decade. One of the magistral directions in this area is a search for the new architectures that suit the specific problems. To name a few: UNet was proposed for segmentation of medical images (Ronneberger et al., 2015); deep convolutional neural networks such as AlexNet (Krizhevsky et al., 2012), VGGNet (Simonyan & Zisserman, 2014), ResNet (He et al., 2015) designed to work with visual data; bidirectional recurrent neural networks for the sequence to sequence tasks (Schuster & Paliwal, 1997; Graves et al., 2013).

There are many problems where it is required to approximate mapping from one function to another, and it is necessary to design problem-specific architectures of neural networks that are adapted to the structure of the problem. Such structures often arise from partial differential equations (PDE) and integral equations (IE). If one has an access to the sequence of right-hand sides and corresponding solutions, the integral operator may be learned on this basis. The only question is to define the structure of the model which approximates the integral operator. It is well-known that integral operators can be approximated well by block low-rank matrices with hierarchical structure (Greengard & Rokhlin, 1987a; Hackbusch, 1999; Tyrtyshnikov, 1996), and one may impose a such constraint on the learning model. Hence we came to the idea to shape the neural network architecture as an extension of hierarchical matrix structure, particularly, the \mathcal{H}^2 -matrix (Hackbusch et al., 2000; Börm, 2010).

In this approach, the forward pass of the neural network is similar to \mathcal{H}^2 matrix by vector multiplication. The proposed architecture inherits the double-tree structure of \mathcal{H}^2 matrices and may be considered as a branching network, like Inception network (Szegedy et al., 2017). However, the summation performed according to the second tree makes the architecture similar to ResNet (He et al., 2015). The resulting network naturally shares the scaling property of \mathcal{H}^2 matrices that may contribute to its performance.

It is worth noting that \mathcal{H}^2 matrix structure is dependent on how one selects close and far regions. Compared to other work on this theme (Fan et al., 2018; 2019) where authors used band matrix for close and tree-to-tree transfer matrices, we considered them as the block-sparse matrices. Our architecture extensively relies on the sparsity template resulting in replacing separate blocks of block-sparse matrices with the sequence of feed-forward fully-connected layers of small size.

In Section 2, we briefly discuss the structure of the \mathcal{H}^2 matrix and describe the architecture of the neural network based on the \mathcal{H}^2 matrix and details of its implementation. Section 3 contains experiments with implemented neural network and a comparison of the proposed neural network with the reference networks. Conducted experiments demonstrate the practical benefits of the proposed architecture and provide a comparison with other existing approaches.

2 NEURAL NETWORK ARCHITECTURE BASED ON \mathcal{H}^2 MATRIX

2.1 FROM FAST MULTIPOLE METHOD (FMM) TO FMMNET

Let us consider two sets of points (point clouds), $x = \{x_i\}_{i=1\dots N}$ and $y = \{y_i\}_{i=1\dots N}$, $x_i, y_i \in \mathbb{R}^d$, where $d = 1, 2, 3$. We are referring to them as source and receiver points respectively. Let us assume that two functions, $q(x)$ and $w(y)$ are defined in subspaces $X, Y \subset \mathbb{R}^d$ so that $x_i \in X$, $y_j \in Y$, and $q_i = q(x_i)$, $w_j = w(y_j)$ for short. Consider the mapping $\phi : q(X) \rightarrow w(Y)$ with $q(X) = \{h_x | h_x = q(x) \forall x \in X\}$ and $w(Y) = \{h_y | h_y = w(y) \forall y \in Y\}$, and our task is to approximate it. The simplest approximation in this regard is a linear transformation $w_j = \sum_{i=1}^N a_{ij} q_i$ with weights a_{ij} which are interactions between i -th and j -th particles; $q(x)$, $w(y)$ and weights a_{ij} are dependent on the problem. One example is the N-body problem, where q_i is a mass of point x_i , w_j is a value of force in point y_j , and a_{ij} is an inverse distance between points x_i and y_j , $a_{ij} = 1/\rho(x_i, y_j)$. Another example is a discretization of some integral equation with a smooth kernel.

Computation of such sum takes $O(N^2)$ operations. However, due to the special structure of the problem, we can approximately evaluate it using the Fast Multipole Method (FMM) in $O(N \ln(1/\varepsilon))$ within a tolerance ε . Detailed information can be found in , but here we are interested only in the computational graph of the algorithm to use it as a basis for neural network architecture.

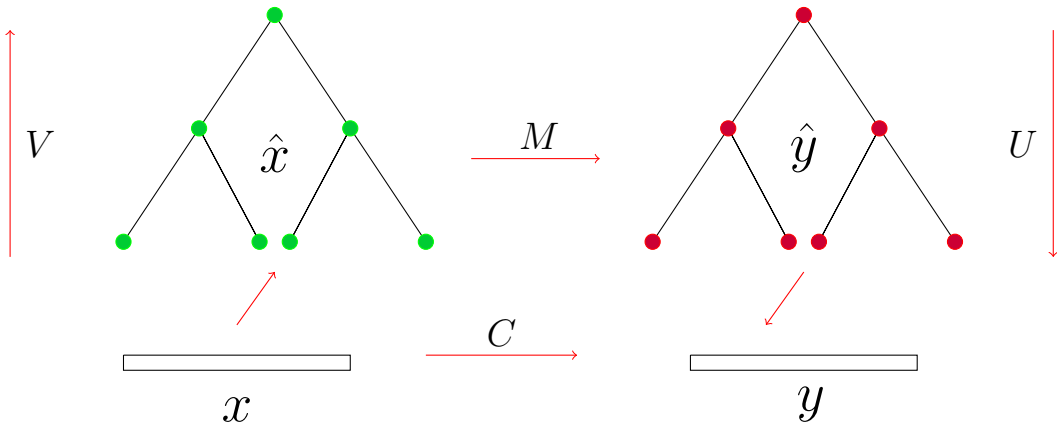


Figure 1: Block cluster trees within FMM matrix by vector product. Each node of a tree denotes vectors, and each junction of nodes corresponds to a linear transformation of them.

The construction of such architecture consists of 2 steps: construction of two block cluster trees according to FMM and generalization of intermediate linear mappings. At first we process geometric information in order to create two cluster trees, and then basing on so-called separability criteria we create a block cluster tree which is stored as a pairwise interaction list. There are many ways to do that, see illustration ... [Huckbush, Tyrtshnikov, Roklin].

To make the second step, we turn our attention to algebraic interpretation of FMM. It can be written using the formalism of \mathcal{H}^2 -matrices in the following form:

$$w = Cq + \sum_{l=L}^1 (U_L \dots U_{L-l+1}) M_l (V_{L-l+1} \dots V_L) q, \quad (1)$$

where $C \in \mathbb{R}^{N \times N}$ is referred to as close interaction matrix, U_l, V_l are interpolator from and projector on the rough grid (transition between so-called levels of decomposition), M_l is a mapping from $q(X)$ to $w(Y)$ on the level $l, l = \overline{1, L}$, w and q are defined on two cloud points X and Y . All matrices included into decomposition 19 have specific structure: U_l and V_l are block-diagonal, C and M_l are block-sparse. The sparsity the pattern of the latter ones is defined by the structure of a certain problem. The corresponding computational graph is presented in Figure 14.

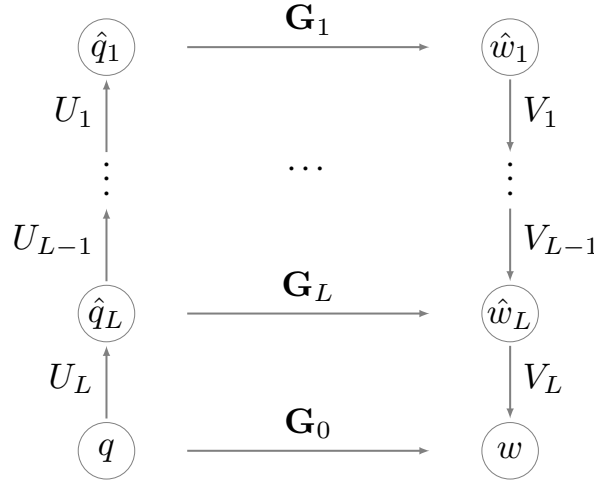


Figure 2: Computational diagram of FMM matrix by vector product. Mappings $G_0, G_l, l = \overline{1, L}$ are linear transformations with matrices C, M_l respectively. In case of FMMNet these mappings are replaced by nonlinear mappings parametrized by neural networks with a certain structure.

2.2 SHAPING THE FMMNET

Having a fixed sparsity pattern obtained on the first step, we substitute linear mappings with more general non-linear maps structured as artificial neural networks. During learning, we assume that coordinates are known and the cluster construction procedure is fixed. For a linear transform, we store linear transformations between the parents and the children of block cluster trees and also linear transformations between the nodes. However, the latter ones are to be replaced by nonlinear mappings in case of FMMNet. The simplest way to do this is to build feedforward neural networks with block sparse linear parts with fixed sparsity patterns. Thus the equation 19 takes the following form:

$$w = \mathbf{G}_0 [q] + \sum_{l=L}^1 (U_L \dots U_{L-l+1}) \mathbf{G}_l [(V_{L-l+1} \dots V_L) q], \quad (2)$$

where $\mathbf{G}_l [z], l = 0 \dots L$ are neural networks with a certain structure which in general may be arbitrary. For example, if one uses fully-connected layer as an elementary unit of such a network, it can be expressed as

$$\mathbf{G}_l [z] = Q_\zeta [Q_{\zeta-1} [\dots Q_1 [z]]], \quad Q_i [t] = f_i [W_i t], \quad (3)$$

where $f_i(t)$ is predefined nonlinearity (for instance, hyperbolic tangent or rectified linear unit), W_i defines linear transformation for i -th layer.

Our idea is to utilize a sparsity pattern of original M_l coming from a certain \mathcal{H}^2 matrix. Block sparse structure of these matrices allows us to split each of them into a set of non-zero blocks supplied by their own nonlinearities:

$$(Q_i [t])_k = f_i \left[\sum_{l \in L_i} h_{kl} [W_{kl} t_l] \right], \quad (4)$$

where k is a number of output vector block, l - number of input vector block, $h_{kl} [z]$ and $f_i [z]$ - nonlinearities, W_{kl} - blocks of matrix, certain number of which are zero-valued.

Another way to introduce non-linearity into the model is to replace each non-zero block of block sparse matrices M_l and C_l with its own non-linear processing unit (e.g., feedforward network).

Therefore, as generalization, we constructed a block sparse layer which preserves the given sparsity template, and it was used as a basic unit for $\mathbf{G}_l [z]$ in our design. We used rectified linear unit (ReLU) as nonlinearity because it is close to a linear transformation and preserves properties that make the model easy to optimize and generalize well (Goodfellow et al., 2016), though any other nonlinear function suited for the learning process may be selected.

It should be noted that we have assumed that the sizes of parameters were defined a priori. As consequence, we propose to use a certain pre-computed \mathcal{H}^2 matrix structure (\mathcal{H}^2 -skeleton) as supplier of related hyperparameters. In practice we propose to use the following strategy:

- If node sets x and y are given for $q(x)$ and $w(y)$, then repeat \mathcal{H}^2 building procedure (??). One should evade to store matrices $C, U_l, V_l, M_l, l = 1 \dots L$ explicitly, because only their sizes are to be used further. We refer to the sequence of such sizes as \mathcal{H}^2 **skeleton**.
- In other case assume that sets x and y are located on tensor grid of the appropriate size and dimension and build \mathcal{H}^2 skeleton for it.

2.3 COMPARISON TO OTHER ARCHITECTURES BASED ON \mathcal{H}^2 -MATRIX

Alternative implementation of \mathcal{H}^2 based neural network is presented in Fan et al. (2019). Authors explored a similar idea to consider \mathcal{H}^2 matrix by vector product as a forward pass of a certain neural network, but the main difference consists in generalization of C and M_l factors. As basic units authors used either locally-connected or convolutional layer. The resulting networks were called as MNN- \mathcal{H}^2 -LC and MNN- \mathcal{H}^2 -mix respectively. However, due to the fact that both locally-connected and convolutional layers are the representations of banded matrices, the MNN- \mathcal{H}^2 -LC and MNN- \mathcal{H}^2 -Mix networks are closer to HSS-matrix based architecture rather than the \mathcal{H}^2 matrix one.

Remark 1. *Hierarchically semiseparable (HSS) matrices (Chandrasekaran et al., 2005; Martinsson & Rokhlin, 2005) are the one dimensional versions of \mathcal{H}^2 matrices.*

Thus MNN- \mathcal{H}^2 -LC network inherits disadvantages of HSS matrices such as memory issues for problems with a significant off-diagonal part in the close matrix. Usage of convolutional layers solved the memory problem in case of MNN- \mathcal{H}^2 -Mix.

In addition, in Section 4 we provide an example of operator that is difficult to be approximated by network of such architecture.

3 COMPUTATIONAL EXPERIMENTS

3.1 IMPLEMENTATION DETAILS

All models and computational experiments were implemented using Python programming language under Anaconda distribution (Analytics, 2015), which includes various pre-built packages for scientific computing. In this study the following packages were used: numpy (Oliphant, 2006), scipy (Jones et al., 2001), matplotlib (Hunter, 2007). The \mathcal{H}^2 -NN model implementation is based on PyTorch package (Paszke et al., 2017); for experiments with MNN-H2 network the source code provided by authors of paper Fan et al. (2018) was used which is available at

<https://github.com/ywfan/mnn-H2> and based on Keras/TensorFlow frameworks (Chollet et al., 2015; Abadi et al., 2015). Some computational experiments are structured as Jupyter Notebooks (Kluyver et al., 2016).

3.2 RADIATIVE TRANSFER EQUATION (RTE)

To compare \mathcal{H}^2 -NN with models proposed in Fan et al. (2019), we considered the one-dimensional Radiative transfer equation (Chandrasekhar, 2013) (RTE):

$$\begin{aligned} v\nabla_x\varphi(x,v) + \mu_t(x,v) &= \mu_s(x)u(x) + f(x), \quad \text{in } \Omega \times \mathcal{S}^{d-1}, \Omega \in \mathbb{R}^d, \\ \varphi(x,v) &= 0, \quad \text{on } \{(x,v) \in \partial\Omega \times \mathcal{S}^{d-1} : n(x)v < 0\}, \\ u(x) &= \frac{1}{4\pi} \int_{\mathcal{S}^{d-1}} \varphi(x,v)dv \end{aligned} \quad (5)$$

Authors of Fan et al. (2018) proposed the way to come from differential form (5) into the integral one,

$$u(x) = \mathcal{I}(\mu_s(x)), \quad \text{or } \mathcal{I} : \mu_s(x) \rightarrow u(x) \quad (6)$$

Having a dataset of paired discretized originals and images $(\mu_s(x_h)^{(i)}, u(x_h)^{(i)})$, $i = 1 \dots N_s$, one may learn the integral mapping using a certain predefined model, for example, parametric model $g(z, \theta)$ with trainable parameters θ . Training process is guided by optimizing specified loss functional that measures quantitatively how output of model with current values of parameters differs from the ground truth:

$$\hat{\theta} = \arg \min_{\theta} \mathcal{L}(u(x_h), g(\mu_s(x_h), \theta)) = \arg \min_{\theta} \frac{1}{N} \sum_{i=1}^N \mathcal{L}_i(u(x_h)^{(i)}, g(\mu_s(x_h)^{(i)}, \theta)) \quad (7)$$

Because both inputs and outputs in this task are real-valued vectors, one may use any loss functional valid for regression-like problems. In this work the squared relative residual was selected in this regard:

$$\mathcal{L}_i(u(x_h)^{(i)}, g(\mu_s(x_h)^{(i)}, \theta)) = \frac{\|u(x_h)^{(i)} - g(\mu_s(x_h)^{(i)}, \theta)\|_F^2}{\|u(x_h)^{(i)}\|_F^2} \quad (8)$$

Dataset for this problem was generated using the source code provided by the authors of paper Fan et al. (2018) (see Section 4.1). All samples were computed on the coinciding sets of sources x and receivers y , $x = y$. For three variants of grid sizes, $N = 320, 640, 1280$ equal number of samples $N_s = 20000$ were generated. To control generalization ability of each model, holdout validation scheme was used with splitting dataset into training and validation parts in the ratio of 2 : 1.

In addition to model proposed in this study, three other ones were selected for comparison, namely simple convolutional model (conv), MNN- \mathcal{H}^2 -Mix and MNN- \mathcal{H}^2 -LC (both from Fan et al. (2018)). All models were trained using the following hyperparameters:

- Optimizer: Adam (Kingma & Ba, 2014)
 - Learning rate: lr = 0.0025,
 - Coefficients used for computing running averages of gradient and its square: $\beta = (0.9, 0.999)$,
 - Term added to the denominator to improve numerical stability $\epsilon = 10^{-5}$,
- Number of layers: $\zeta = 3$,
- Nonlinearity: ReLU,
- Number of iterations: $N_{it} = 2000$,
- Model initialization: Glorot uniform initializer, also known as Xavier uniform initializer (Glorot & Bengio, 2010).

Figure 3 displays learning process it terms of evolving loss functional. Average values of time per iteration presented in Table ??.

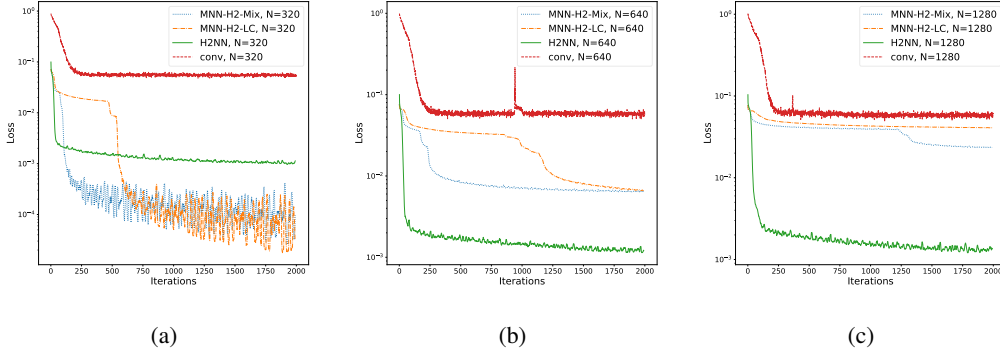


Figure 3: Loss decrease during optimization process for RTE 1D with different grid sizes N : (a) $N = 320$; (b) $N = 640$; (c) $N = 1280$. Curves legend: dotted blue line for multiscale neural network based on hierarchical nested bases with convolutional and locally-connected layers (MNN-H2-Mix); dash-dotted orange line for multiscale neural network based on hierarchical nested bases with locally-connected layers (MNN-H2-LC); solid green line for \mathcal{H}^2 -based neural network (H2NN, proposed approach); dashed red for simple convolutional network (conv).

In comparison to proposed network, both MNN- \mathcal{H}^2 -Mix and MNN- \mathcal{H}^2 -LC converged faster to the lower values of loss functional in case of $N = 320$. But for higher dimensionality these models saturated to larger loss values while proposed model quickly decreased to lower ones. As expected, simple but not specific network showed the worst performance for all considered dimensions. These observations suggest evidence that \mathcal{H}^2 -NN model is more scalable. Table 1 contains information about train and validation errors (mean relative residuals) after $N_{it} = 2000$ iterations.

N	h2nn	MNN- \mathcal{H}^2 -Mix	MNN- \mathcal{H}^2 -LC	conv
320	0.02350/0.02346	0.01197/0.01196	0.00366/0.00383	0.19538/0.19359
640	0.02676/0.02687	0.06179/0.06381	0.06271/0.06692	0.19683/0.19671
1280	0.03240/0.03233	0.12397/0.125108	0.16229/0.16438	0.19686/0.19552

Table 1: RTE 1D, comparison of mean relative residual errors for different methods and grid sizes $N = 320, 640, 1280$. Each cell is formatted as $\varepsilon_{\text{train}}/\varepsilon_{\text{test}}$, where $\varepsilon_{\text{train}}$ and $\varepsilon_{\text{test}}$ are mean relative residual errors measured on training and test sets.

Mean relative residuals measured on validation part of datasets as well as memory consumption of considered models are shown in Figure 4.

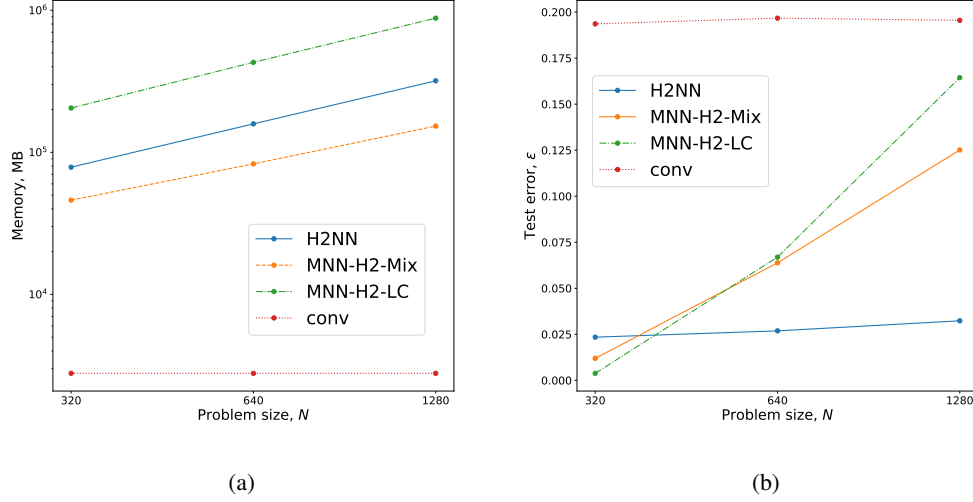


Figure 4: Memory and error comparison of \mathcal{H}^2 -NN, MNN- \mathcal{H}^2 -Mix and MNN- \mathcal{H}^2 -LC models. (a) memory required for the model storage; (b) test error

According to Figure 4, proposed architecture (\mathcal{H}^2 -NN) has the best scalability with moderate memory consumption, surpassed only by MNN- \mathcal{H}^2 -Mix model.

3.3 CUSTOM OPERATOR EXAMPLE

It is known that convolution operation may be represented as multiplication by Toeplitz matrix. Experience shows (Fan et al., 2019) that \mathcal{H}^2 -inspired architectures with convolutional layers (MNN- \mathcal{H}^2 -Mix) are good approximators for matrices structured closely to Toeplitz ones. A natural question is how well it capture more general dependencies. We considered the following weights:

$$a_{ij} = \frac{1}{\|x_i - y_j\|} f(i, j), \quad (9)$$

where $f(i, j) = \frac{(x_i + y_j)^2}{N^5}$.

Inputs were similar to ones used in section 3.2, and outputs were generated by this custom weighting procedure. The same setup as in previous section was used to train and validate conv, MNN- \mathcal{H}^2 -Mix/LC and \mathcal{H}^2 -net models. Training procedure is visualised in Figure 5. Average values of time per iteration presented in Table ???. Mean residual errors and memory consumption of models are shown in Figure 6.

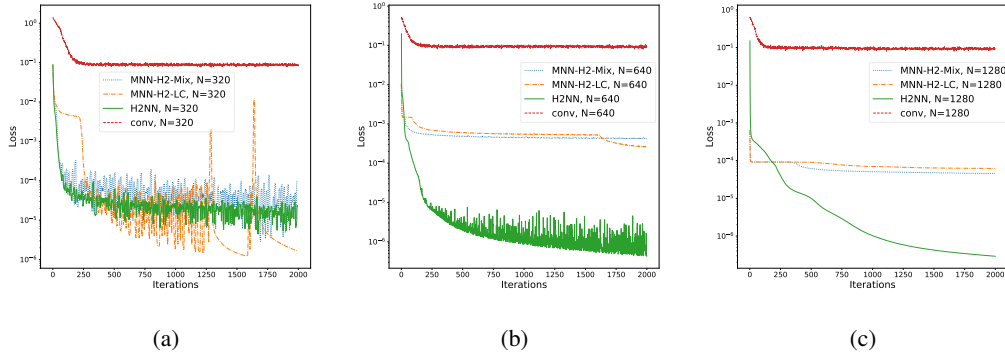


Figure 5: Loss decrease during optimization process for custom operator example with different grid sizes N : (a) $N = 320$; (b) $N = 640$; (c) $N = 1280$. Curves legend: dotted blue line for multiscale neural network based on hierarchical nested bases with convolutional and locally-connected layers (MNN-H2-Mix); dash-dotted orange line for multiscale neural network based on hierarchical nested bases with locally-connected layers (MNN-H2-LC); solid green line for \mathcal{H}^2 -based neural network (H2-NN, proposed approach); dashed red for simple convolutional network (conv).

N	h2nn	MNN- \mathcal{H}^2 -Mix	MNN- \mathcal{H}^2 -LC	conv
320	0.00790/0.00789	0.00857/0.00858	0.00218/0.00218	0.26599/0.26600
640	0.00424/0.00425	0.14413/0.14592	0.10721/0.11022	0.27551/0.27860
1280	0.01464/0.00425	0.19069/0.19070	0.22265/0.22287	0.33206/0.33301

Table 2: Custom operator example, comparison of mean relative residual errors for different methods and grid sizes $N = 320, 640, 1280$. Each cell is formatted as $\varepsilon_{\text{train}}/\varepsilon_{\text{test}}$, where $\varepsilon_{\text{train}}$ and $\varepsilon_{\text{test}}$ are mean relative residual errors measured on training and test sets.

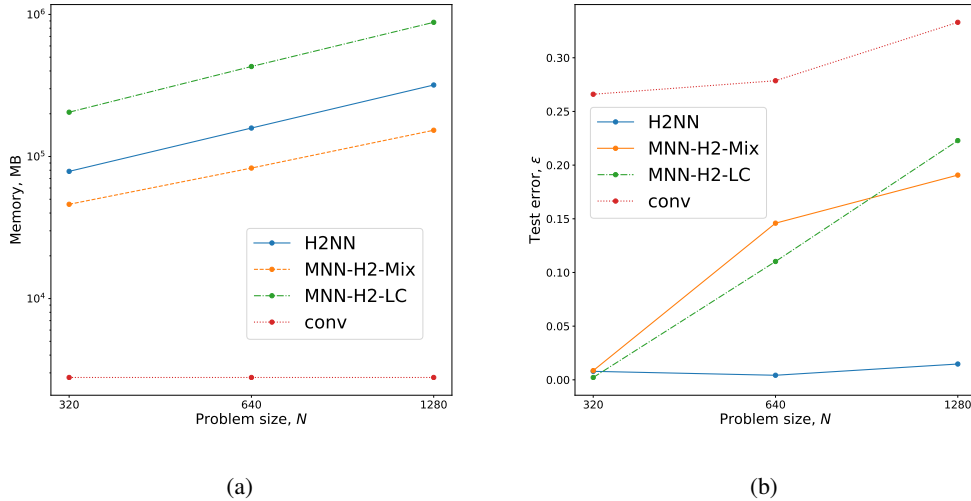


Figure 6: Memory and error comparison of \mathcal{H}^2 -NN, MNN- \mathcal{H}^2 -Mix and MNN- \mathcal{H}^2 -LC models. (a) memory required for the model storage; (b) test error

MNN- \mathcal{H}^2 -Mix showed nearly comparable with MNN- \mathcal{H}^2 -LC model behaviour, though had better performance for lower problem size, $N = 320$ (Figure 5, (a); Table 2). However, both models were

outperformed by \mathcal{H}^2 -NN model in higher dimensions, $N = 640, 1280$ (Figure 5, (b), (c); Table 2). Memory consumption preserved the trend outlined in the previous section.

4 RELATED WORK

Structured low-rank matrix formats are actively used to solve partial differential equations (PDEs) and integral equations (IEs) (Greengard & Rokhlin, 1987a; Tyrtshnikov, 1996; Bebendorf & Hackbusch, 2003; Bardhan et al., 2009). Some of them were intentionally designed to reduce memory and computational costs. Being the particular example of such formats, \mathcal{H} -matrices (Hackbusch, 1999) together with mosaic-skeleton ones (Tyrtshnikov, 1996) allow to store dense matrices by $\mathcal{O}(N \log N)$ memory cost and to perform matrix-vector multiplication by $\mathcal{O}(N \log N)$ operations. \mathcal{H}^2 matrices (Hackbusch et al., 2000; Börm, 2010; Bebendorf & Venn, 2012) which are the central point of the fast multipole method (FMM) and additionally reduce these costs to $\mathcal{O}(N)$. At the same time, solving the linear system with \mathcal{H} and \mathcal{H}^2 matrix is challenging. The complicated structure of block low-rank matrices makes it hard to build a direct solver. Another issue regarding the direct solution is preserving the $\mathcal{O}(N)$ memory complexity during computations. Despite the theoretical knowledge that \mathcal{H}^2 matrices (with certain conditions) have \mathcal{H}^2 matrix as an inverse (Bebendorf & Hackbusch, 2003; Bebendorf, 2005), the implementation of the \mathcal{H}^2 direct solver is a work in progress.

The rapidly growing area of artificial neural networks allowed to propose differently approaches to the solution of PDEs (Lagaris et al., 1998; Chiamonte & Kiener, 2013; Baymani et al., 2010) and IEs (Elshafey et al., 1991; Vemuri & Jang, 1991; Effati & Buzhabadi, 2012). In general, the main idea is to teach a neural network to act as a transformation of the right-hand side to the solution. Theoretical results state that neural networks are universal approximators of functional dependencies: according to Cybenko theorem (universal approximation theorem) (Hornik et al., 1989; Hornik, 1991), feed-forward network with 2 layers (one hidden layer) of finite sizes and mildly restricted nonlinearity is a universal approximator for continuous functions on compact sets in \mathbb{R}^d . However, in many practical applications such as speech recognition, image segmentation, generative modelling, multi-layered as well as non-feedforward architectures are actively used.

Typical architecture used for solving PDE and IE is a feedforward network with a single hidden layer (Chiamonte & Kiener, 2013; Baymani et al., 2010; Elshafey et al., 1991; Vemuri & Jang, 1991; Piscopo et al., 2019; Effati & Buzhabadi, 2012) or with multi-layered structure (Ramchoun et al., 2016; Lagaris et al., 1998). These models have fully-connected layers with dense unstructured matrices leading to memory issues.

The idea of construction \mathcal{H} -, \mathcal{H}^2 -based neural networks is not unique, and several implementations of it are known Fan et al. (2018; 2019) where authors used band matrix for close and tree-to-tree transfer matrices. This paper develops the idea of \mathcal{H}^2 -NN architecture, proposing a new method of layers construction and showing on practice benefits of this method.

5 CONCLUSIONS

In this work, we proposed a new \mathcal{H}^2 -based architecture and showed its benefits over the existing analogs.

In the context of partial differential and integral equations used for modeling physical processes, machine learning holds the promise of being able to capture relationships between observable measurements in complicated conditions (e.g., complex geometry). Moreover, trainable parametric models may potentially generalize to various input conditions. In that case, neural network architectures inspired by established constructions like \mathcal{H}^2 -matrices would be easier to analyze.

It is worth noting that a common problem for every neural network-based method for solving PDEs and IEs is a large learning time. However, as soon as the network is trained, the solution is to be computed quickly by one forward pass. Since training is required at once, such an approach is prospective in case of a large number of typical problems with the shared operator and different right-hand sides.

In future work, we will continue researching \mathcal{H}^2 -networks generated by block-sparsity patterns emerging in \mathcal{H}^2 -matrices. Complementary to problems that arise in mathematical physics, \mathcal{H}^2 -networks seem to be applicable in conventional machine learning problems.

REFERENCES

- Martín Abadi, Ashish Agarwal, Paul Barham, Eugene Brevdo, Zhifeng Chen, Craig Citro, Greg S. Corrado, Andy Davis, Jeffrey Dean, Matthieu Devin, Sanjay Ghemawat, Ian Goodfellow, Andrew Harp, Geoffrey Irving, Michael Isard, Yangqing Jia, Rafal Jozefowicz, Lukasz Kaiser, Manjunath Kudlur, Josh Levenberg, Dandelion Mané, Rajat Monga, Sherry Moore, Derek Murray, Chris Olah, Mike Schuster, Jonathon Shlens, Benoit Steiner, Ilya Sutskever, Kunal Talwar, Paul Tucker, Vincent Vanhoucke, Vijay Vasudevan, Fernanda Viégas, Oriol Vinyals, Pete Warden, Martin Wattenberg, Martin Wicke, Yuan Yu, and Xiaoqiang Zheng. TensorFlow: Large-scale machine learning on heterogeneous systems, 2015. URL <https://www.tensorflow.org/>. Software available from tensorflow.org.
- Continuum Analytics. Anaconda software distribution. Computer software. Vers. 2-2.4.0., Nov. 2015. URL <https://continuum.io>.
- Jaydeep Bardhan, Michael Altman, Bruce Tidor, and Jacob White. “reverse-schur” approach to optimization with linear PDE constraints: Application to biomolecule analysis and design. *J. Chem. Theory Comput.*, 5(12):3260–3278, 2009.
- Modjtaba Baymani, Asghar Kerayechian, and Sohrab Effati. Artificial neural networks approach for solving stokes problem. *Applied Mathematics*, 1(04):288, 2010.
- Mario Bebendorf. Hierarchical LU decomposition-based preconditioners for BEM. *Computing*, 74(3):225–247, 2005.
- Mario Bebendorf and Wolfgang Hackbusch. Existence of \mathcal{H} -matrix approximants to the inverse FE-matrix of elliptic operators with L^∞ -coefficients. *Numer. Math.*, 95(1):1–28, 2003.
- Mario Bebendorf and Raoul Venn. Constructing nested bases approximations from the entries of non-local operators. *Numer. Math.*, 121(4):609–635, 2012.
- Steffen Börm. *Efficient numerical methods for non-local operators: \mathcal{H}^2 -matrix compression, algorithms and analysis*, volume 14. European Mathematical Society, 2010.
- S Chandrasekaran, M Gu, and W Lyons. A fast adaptive solver for hierarchically semiseparable representations. *Calcolo*, 42(3-4):171–185, 2005.
- Subrahmanyam Chandrasekhar. *Radiative transfer*. Courier Corporation, 2013.
- MM Chiramonte and M Kiener. Solving differential equations using neural networks. *Machine Learning Project*, 2013.
- François Chollet et al. Keras. <https://keras.io>, 2015.
- Sohrab Effati and Reza Buzhabadi. A neural network approach for solving fredholm integral equations of the second kind. *Neural Computing and Applications*, 21(5):843–852, 2012.
- I Elshafiey, L Udpa, and SS Udpa. A neural network approach for solving integral equations. In 1991., *IEEE International Symposium on Circuits and Systems*, pp. 1416–1419. IEEE, 1991.
- Yuwei Fan, Lin Lin, Lexing Ying, and Leonardo Zepeda-Núñez. A multiscale neural network based on hierarchical matrices. *arXiv preprint arXiv:1807.01883*, 2018.
- Yuwei Fan, Jordi Feliu-Faba, Lin Lin, Lexing Ying, and Leonardo Zepeda-Núñez. A multiscale neural network based on hierarchical nested bases. *Research in the Mathematical Sciences*, 6(2): 21, 2019.
- Xavier Glorot and Yoshua Bengio. Understanding the difficulty of training deep feedforward neural networks. In *Proceedings of the thirteenth international conference on artificial intelligence and statistics*, pp. 249–256, 2010.

-
- Ian Goodfellow, Yoshua Bengio, and Aaron Courville. *Deep Learning*. MIT Press, 2016. <http://www.deeplearningbook.org>.
- Alex Graves, Abdel-rahman Mohamed, and Geoffrey Hinton. Speech recognition with deep recurrent neural networks. In *2013 IEEE international conference on acoustics, speech and signal processing*, pp. 6645–6649. IEEE, 2013.
- L. Greengard and V. Rokhlin. A fast algorithm for particle simulations. *J. Comput. Phys.*, 73(2):325–348, December 1987a.
- Leslie Greengard and Vladimir Rokhlin. A fast algorithm for particle simulations. *Journal of computational physics*, 73(2):325–348, 1987b.
- Leslie Greengard, Jingfang Huang, Vladimir Rokhlin, and Stephen Wandzura. Accelerating fast multipole methods for the helmholtz equation at low frequencies. *IEEE Computational Science and Engineering*, 5(3):32–38, 1998.
- W. Hackbusch, B.N. Khoromskij, and S. Sauter. On \mathcal{H}^2 -matrices. In *H.-J. Bungartz, et al. (eds.), Lectures on Applied Mathematics*, pp. 9–30. Springer-Verlag, Berlin Heidelberg, 2000.
- Wolfgang Hackbusch. A sparse matrix arithmetic based on \mathcal{H} -matrices. part i: Introduction to \mathcal{H} -matrices. *Computing*, 62(2):89–108, 1999.
- Kaiming He, Xiangyu Zhang, Shaoqing Ren, and Jian Sun. Deep residual learning for image recognition. *arXiv preprint arXiv:1512.03385*, 2015.
- Kurt Hornik. Approximation capabilities of multilayer feedforward networks. *Neural networks*, 4(2):251–257, 1991.
- Kurt Hornik, Maxwell Stinchcombe, and Halbert White. Multilayer feedforward networks are universal approximators. *Neural networks*, 2(5):359–366, 1989.
- John D Hunter. Matplotlib: A 2D graphics environment. *Computing in science & engineering*, 9(3):90–95, 2007. doi: 10.1109/MCSE.2007.55.
- Eric Jones, Travis Oliphant, Pearu Peterson, et al. SciPy: Open source scientific tools for Python, 2001. URL <http://www.scipy.org/>. [Online; accessed December 27, 2022].
- Diederik P Kingma and Jimmy Ba. Adam: A method for stochastic optimization. *arXiv preprint arXiv:1412.6980*, 2014.
- Thomas Kluyver, Benjamin Ragan-Kelley, Fernando Pérez, Brian Granger, Matthias Bussonnier, Jonathan Frederic, Kyle Kelley, Jessica Hamrick, Jason Grout, Sylvain Corlay, Paul Ivanov, Damián Avila, Safia Abdalla, and Carol Willing. Jupyter notebooks – a publishing format for reproducible computational workflows. In F. Loizides and B. Schmidt (eds.), *Positioning and Power in Academic Publishing: Players, Agents and Agendas*, pp. 87 – 90. IOS Press, 2016. doi: 10.3233/978-1-61499-649-1-87.
- Alex Krizhevsky, Ilya Sutskever, and Geoffrey E Hinton. Imagenet classification with deep convolutional neural networks. In *Advances in neural information processing systems*, pp. 1097–1105, 2012.
- Isaac E Lagaris, Aristidis Likas, and Dimitrios I Fotiadis. Artificial neural networks for solving ordinary and partial differential equations. *IEEE transactions on neural networks*, 9(5):987–1000, 1998.
- Per-Gunnar Martinsson and Vladimir Rokhlin. A fast direct solver for boundary integral equations in two dimensions. *J. Comput. Phys.*, 205(1):1–23, 2005.
- Travis E Oliphant. *A guide to NumPy*, volume 1. Trelgol Publishing USA, 2006.
- Adam Paszke, Sam Gross, Soumith Chintala, Gregory Chanan, Edward Yang, Zachary DeVito, Zeming Lin, Alban Desmaison, Luca Antiga, and Adam Lerer. Automatic differentiation in pytorch. *openreview.net*, 2017.

- Maria Laura Piscopo, Michael Spannowsky, and Philip Waite. Solving differential equations with neural networks: Applied to the calculation of cosmological phase transitions. *arXiv preprint arXiv:1902.05563*, 2019.
- Hassan Ramchoun, Mohammed Amine Janati Idrissi, Youssef Ghanou, and Mohamed Ettaouil. Multilayer perceptron: Architecture optimization and training. *IJIMAI*, 4(1):26–30, 2016.
- Olaf Ronneberger, Philipp Fischer, and Thomas Brox. U-net: Convolutional networks for biomedical image segmentation. In *International Conference on Medical image computing and computer-assisted intervention*, pp. 234–241. Springer, 2015.
- Mike Schuster and Kuldip K Paliwal. Bidirectional recurrent neural networks. *IEEE Transactions on Signal Processing*, 45(11):2673–2681, 1997.
- Karen Simonyan and Andrew Zisserman. Very deep convolutional networks for large-scale image recognition. *arXiv preprint arXiv:1409.1556*, 2014.
- Christian Szegedy, Sergey Ioffe, Vincent Vanhoucke, and Alexander A Alemi. Inception-v4, inception-resnet and the impact of residual connections on learning. In *Thirty-First AAAI Conference on Artificial Intelligence*, 2017.
- E. E. Tyrtshnikov. Mosaic-skeleton approximations. *Calcolo*, 33(1):47–57, 1996. doi: 10.1007/BF02575706.
- V Rao Vemuri and Gyu-Sang Jang. Neural networks for fredholm-type integral equations. In *Applications of Artificial Neural Networks II*, volume 1469, pp. 563–574, 1991.
- Roy Williams. Unification of spectral and inertial bisection. *Techn. Rep., Caltech*, 1994.

A APPENDIX: BASIC CONCEPTS OF \mathcal{H}^2 MATRIX

In general, computation of matrix by vector product requires $\mathcal{O}(N^2)$ operations. and storage of corresponding matrix requires $\mathcal{O}(N^2)$ items of memory. However, additional knowledge about the problem may reduce the computation and storage complexity to $\mathcal{O}(N)$.

A.1 SEPARATION PROPERTY

Low-rank matrices is an example of structured matrices that have reduced number of parameters, $\mathcal{O}(2NR)$, where R is a matrix rank, and $R < N$. Due to its compressing property, low-rank assumption is widely used in many applications of computational science. Matrix A from equation ?? also shares the low-rank constraint if sets x and y are **spatially separated**. We refer to this assumption as separation property of the problem.

Remark 2. *Spatial separation implies that the distance $\rho(x_c, y_c)$ between centers x_c and y_c of the bounding boxes of sets x and y is larger than some constant ϱ scaled by the size of bounding boxes α_{bb} .*

$$\rho(x_c, y_c) > \varrho \alpha_{bb} \quad (10)$$

The assumptions is valid for N-body problem as well as for IEs with smooth kernels Greengard & Rokhlin (1987b); Greengard et al. (1998).

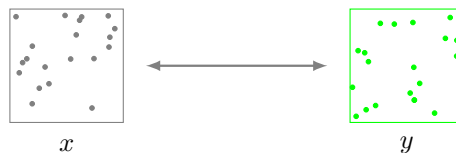


Figure 7: Example of sets that share separation property: two sets x and y that have bounding boxes distant enough from each other

A.2 HIERARCHICAL GRID

In general case sets x and y are not spatially separated in a straight way. Moreover, in many problems these sets are coincident, thus a separation property does not hold for matrix A directly. However, one may consider subsets of x and y , and for some pairs of these subsets the spatial separation property is valid. Consequently, there are submatrices (blocks) of matrix A with low-rank. That is the basic idea behind block low-rank matrices.

The natural way to obtain subsets is to split sets x and y into η sub-blocks **hierarchically**. Sets x and y are separated into η arbitrary equal subsets (Williams, 1994). Then each subset is recursively separated into its η subsets until the stopping criteria is reached.

Example A.1. As an example consider x and y on the same uniform tensor grid in $2d$. We separate squares into four equal sub-squares ($\eta = 4$), see Figure 8a. The number of boxes on level l of the grid is $H_l = \eta^l$.

Remark 3. Enumeration of $2d/3d$ clouds of points is crucial to constitute sets x and y . Essentially, one should provide a rule for conversion of coordinate arrays into flat indices. This operation is equal to the permutation of vectors q and w , and rows and columns of matrix A . The standard convention is a depth-first box-wise numeration.

A.3 CLOSE AND FAR BLOCKS

In \mathcal{H}^2 matrices, nested grid can be subdivided into regions of two types at each level. Consider the level with the smallest box size, $l = L$, and let us look closer at the structure of source and receiver vectors. The former one contains the following blocks:

$$\tilde{q}_i = q(\tilde{x}_i), i \in 1 \dots H_L, \tilde{w}_j = w(\tilde{y}_j), j \in 1 \dots H_L,$$

where $\tilde{q}_i, \tilde{w}_j \in \mathbb{R}^B$, B is block size, H_L is number of blocks on level L . Thus,

$$q = \begin{bmatrix} \tilde{q}_1 \\ \vdots \\ \tilde{q}_{H_L} \end{bmatrix}, w = \begin{bmatrix} \tilde{w}_1 \\ \vdots \\ \tilde{w}_{H_L} \end{bmatrix}, A = \begin{bmatrix} A_{11} & \dots & A_{1H_L} \\ \vdots & \ddots & \vdots \\ A_{H_L1} & \dots & A_{H_L} \end{bmatrix},$$

where $A_{ij} \in \mathbb{R}^{B \times B}$.

For each receiver box $\tilde{y}_i, i \in 1 \dots H_L$ let us consider set of sources boxes \tilde{x}_j within the circle of radius $\rho = \varrho \alpha_L$, where ϱ is a predefined constant, α_L is a box size on level L .

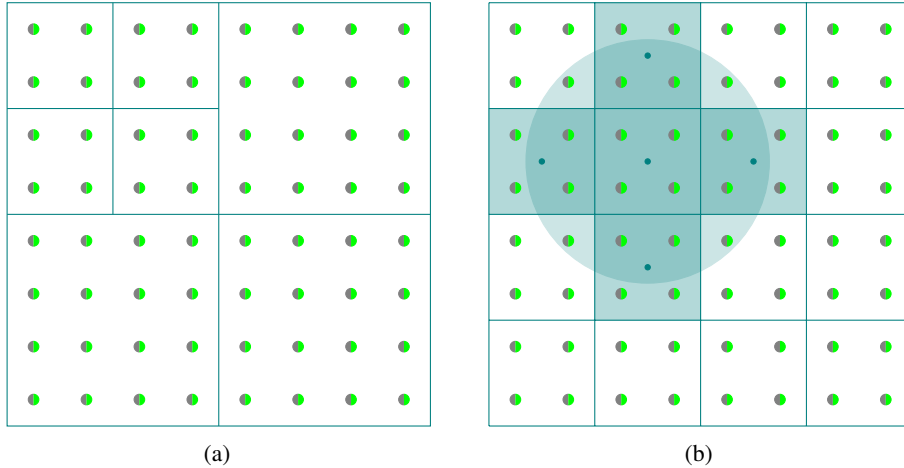


Figure 8: Grid operations in two-dimensional case: (a) hierarchical nested division into blocks; (b) close-far assignments to the blocks at the same level. Close blocks are highlighted by blue color. The latter operation may be performed in various ways.

In case of receivers close to sources, corresponding blocks $A_{ij} \in \mathbb{R}^{B \times B}$ of matrix A have **no low-rank** since spatial separation property does not hold for them. Because they correspond to closer interactions, we call them **close blocks**. On the level $l = L$ these close blocks constitute close matrix C , see Figure 9. Remaining blocks called **far blocks** can be approximated well with low-rank. The far blocks constitute **far matrix** F_L , see Figure 10. Thus the level L structure of \mathcal{H}^2 matrix-by-vector product can be rewritten as

$$w = Aq = Cq + F_L q \quad (11)$$

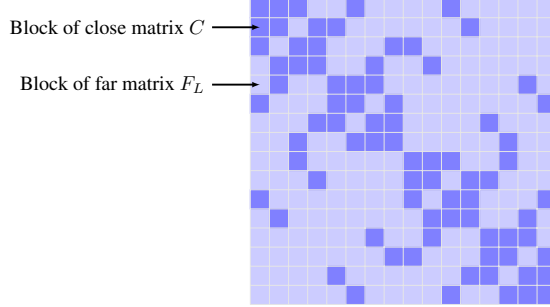


Figure 9: Example of \mathcal{H}^2 matrix $A = C + F_L$, $L = 4$. Far and close blocks are highlighted by light and dark blue colors respectively.

A.4 BOTTOM-LEVEL COMPRESSION

Owing to separation property, each far block $F_{ij} \in \mathbb{R}^{B \times B}$ of far matrix F_L has a low rank:

$$F_{ij} \approx \tilde{U}_i \tilde{F}_{ij} \tilde{V}_j, \quad \forall i, j \in 1, \dots, H_L, \quad (12)$$

where $\tilde{F}_{ij} \in \mathbb{R}^{r \times r}$ is a compressed far block, matrices $\tilde{U}_i \in \mathbb{R}^{B \times r}$ and $\tilde{V}_j \in \mathbb{R}^{r \times B}$ are rectangular compression matrices.

The key assumption of \mathcal{H}^2 matrix is that all the blocks in i -th row have the same left rectangular compression factor \tilde{U}_i and all blocks in j -th column have the same rectangular compression right factor \tilde{V}_j^T . The goal of the compression procedure is to sparsify the matrix A by obtaining compressed blocks \tilde{F}_{ij} instead of original blocks F_{ij} .

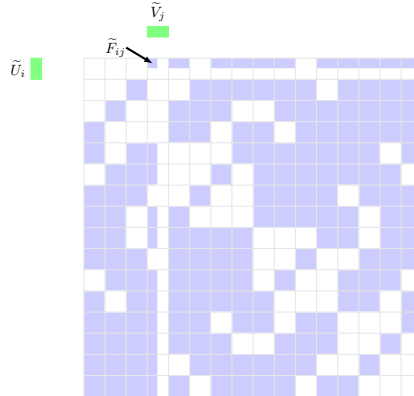


Figure 10: Matrix F_L , $L = 4$ that contains far blocks of \mathcal{H}^2 matrix. Decomposition of pointed block F_{ij} into $\tilde{U}_i \tilde{F}_{ij} \tilde{V}_j^T$ product allows to compress it; matrices \tilde{U}_i , \tilde{V}_j are assumed to be common for every block of i -th row and j -th column respectively.

We introduce the block-diagonal rectangular compression matrix

$$U_L = \begin{bmatrix} \tilde{U}_1 & 0 & 0 \\ 0 & \ddots & 0 \\ 0 & 0 & \tilde{U}_M \end{bmatrix}, \quad (13)$$

where $U_L \in \mathbb{R}^{BH_L \times rH_L}$. Similarly, for block columns, we obtain the block-diagonal rectangular compression matrix

$$V_L = \begin{bmatrix} \tilde{V}_1 & 0 & 0 \\ 0 & \ddots & 0 \\ 0 & 0 & \tilde{V}_M \end{bmatrix}, \quad (14)$$

where $V_L \in \mathbb{R}^{rH_L \times BH_L}$. For the far matrix, we obtain the factorization

$$F_L = U_L \widehat{M}_L V_L,$$

where $\widehat{M}_L \in \mathbb{R}^{rH_L \times rH_L}$ is a compressed far matrix. Thus, for the A we obtain

$$w = Cq + U_L \widehat{M}_L V_L q, \quad (15)$$

see Figure 11.

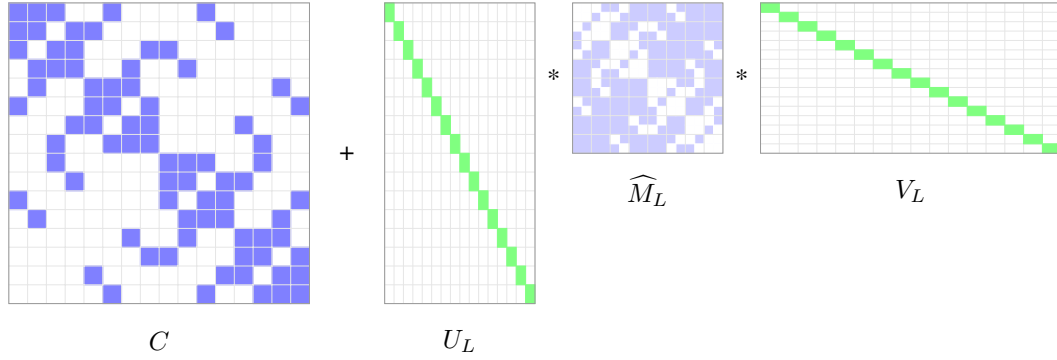


Figure 11: \mathcal{H}^2 matrix, compression at last level, L . C matrix captures close interaction blocks, \widehat{M}_L is a compressed far interaction matrix, U_L and V_L are block diagonal compressing matrices.

Consider the matrix \widehat{M}_L ; our next goal is to compress this matrix. In order to do that, we move to level $l = L - 1$. On this level blocks are united in groups of η .

Take a look at receiver boxes that are close to source boxes on the current level. We say that they set the **interaction list**.

Definition A.1. A far block is in interaction list on level l if the block that contains it on level $l - 1$ is a close block, see Figure 12. Blocks that correspond to interaction list on level l constitute the interaction list matrix M_{l+1} .

We separate \widehat{M}_L into two parts: the interaction list matrix M_L , and compressible matrix F_{L-1} , see Figure 12.

$$\widehat{M}_L = M_L + F_{L-1}. \quad (16)$$

Therefore,

$$F_L = U_L \widehat{M}_L V_L = U_L M_L V_L + U_L F_{L-1} V_L \quad (17)$$

Thus, we obtain:

$$w = Cq + U_L M_L V_L q + U_L F_{L-1} V_L q. \quad (18)$$

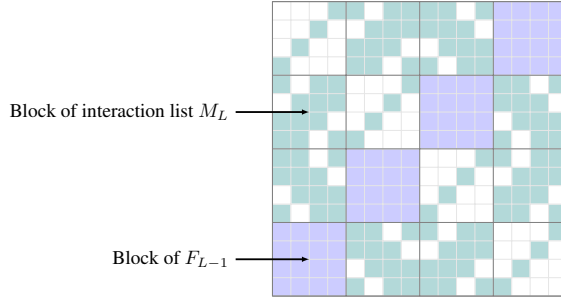


Figure 12: \mathcal{H}^2 matrix, further decomposition of matrix \widehat{M}_L into sum of close and far interaction matrices M_L and F_{L-1} . Close blocks are denoted by cyan color, far blocks are illustrated by blue color. White colored blocks are zero-valued.

A.5 COMPRESSION AT NEXT LEVELS

For far blocks F_{L-1} from level $l = L - 1$, we compute the compression matrices U_{L-1} and V_{L-1} , by the analogy to level $l = L$. Repeating till the level $l = 1$ we obtain the final formula:

$$w = Cq + \sum_{l=L}^1 (U_L \dots U_{L-l+1}) M_l (V_{L-l+1} \dots V_L) q. \quad (19)$$

A.6 \mathcal{H}^2 MATRIX BY VECTOR PRODUCT

Let us describe the \mathcal{H}^2 matrix by vector multiplication procedure. Matrix \mathcal{H}^2 is given by equation (19)

Input: Matrices $C, U_l, V_l, M_l, l = 1 \dots L$, vector q

Output: Vector w defined by equation (19)

$w = 0$

$\hat{w}_l = 0, l = 1 \dots L$

$w = w + Cq$

for $l \leftarrow 1$ **to** L **do**

for $i \leftarrow L$ **to** $L + 1 - l$ **do**

$\hat{q}_i = V_i \hat{q}_{i+1}$ ($\hat{q}_{L+1} = q$)

end

$\hat{w}_l = \hat{w}_l + M_l \hat{q}_l$;

for $i \leftarrow l$ **to** L **do**

$\hat{w}_{i+1} = \hat{w}_{i+1} + U_i \hat{w}_i$ ($\hat{w}_{L+1} = w$)

end

end

Algorithm 1: Pseudo-code for computation of \mathcal{H}^2 matrix by vector product

In Figure 13 the illustration of Algorithm 1 is shown. Vectors are placed in circles, arrows represent the matrix by vector product.

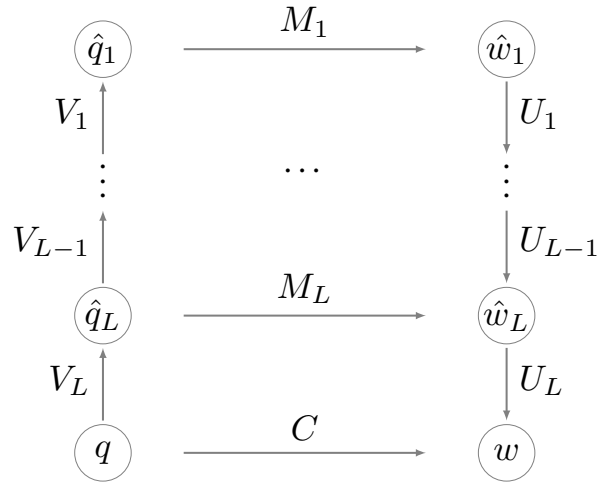


Figure 13: Computational diagram of \mathcal{H}^2 matrix by vector product

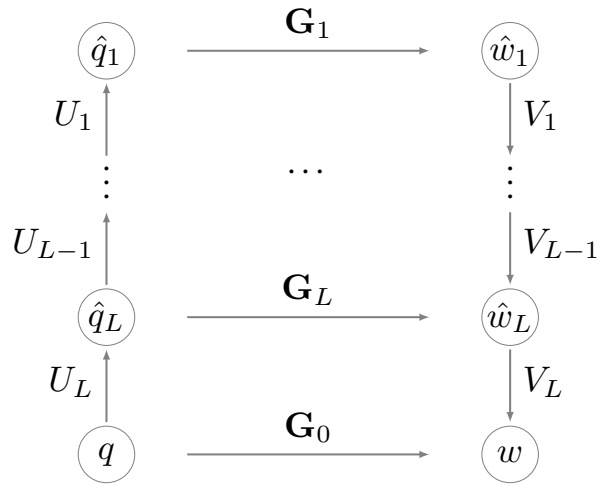


Figure 14: Computational diagram of \mathcal{H}^2 -based neural network